Bull. Mater. Sci., Vol. 37, No. 6, October 2014, pp. 1477–1483. © Indian Academy of Sciences.

Boron-doped MnTe semiconductor-sensitized ZnO solar cells

AUTTASIT TUBTIMTAE[a,*], SUWANNA SHEANGLIW[a], KRITSADA HONGSITH[b,c] and SUPAB CHOOPUN[b,c]

[a]Department of Physics, Faculty of Liberal Arts and Science, Kasetsart University, Kamphaeng Saen Campus, Nakhon Pathom 73140, Thailand
[b]Department of Physics and Material Sciences, Faculty of Science, Chiang Mai University, Chiang Mai 50200, Thailand
[c]Thailand Center of Excellence in Physics (ThEP Center), CHE, Bangkok 10400, Thailand

MS received 24 July 2013

Abstract. We studied the photovoltaic performance of boron-doped MnTe semiconductor-sensitized solar cells (B-doped MnTe SSCs). The B-doped MnTe semiconductor was grown on ZnO using two stages of the successive ionic layer adsorption and reaction (SILAR) technique. The two phases of B-doped semiconductor nanoparticles (NPs), i.e. MnTe and $MnTe_2$ were observed with a diameter range of approximately 15–30 nm. The result of the energy conversion efficiency of the sample with boron doping was superior compared to that of an undoped sample, due to the substantial change in the short-circuit current density and the open-circuit voltage. In addition, plots of $(\alpha h\nu)^2$ vs $h\nu$ with band gaps of 1·30 and 1·27 eV were determined for the undoped and B-doped MnTe NPs, respectively. It can be noted that the boron doping effects with the change in the band gap and lead to an improvement in the crystalline quality and also intimate contact between the larger sizes of MnTe NPs. Hence, a noticeably improved photovoltaic performance resulted. However, this kind of semiconductor sensitizer can be further extended by experiments on yielding a higher power conversion efficiency and greater stability of the device.

Keywords. Manganese telluride; boron doping; successive ionic layer adsorption and reaction (SILAR); solar cell.

1. Introduction

The wide-band gap metal oxide, ZnO, is one of the most important oxide semiconducting materials and has been used widely in many applications and forms many types of well-aligned one-dimensional ZnO nanostructures, such as photocatalysts (Georgekutty *et al* 2008), ultraviolet laser diodes (Okazaki *et al* 2011), optical switches (Mu *et al* 2011) and solar cells (Wang *et al* 2010; Majidi and Baxter 2011; Zhu *et al* 2011), because of its wide band gap (~ 3·3 eV) and exciton binding energy (~ 60 meV), as well its cheap price, versatility and the possibility of large scale production using non-toxic materials (Kahn *et al* 2005; Ravirajan *et al* 2006). ZnO has better electron mobility than TiO_2. The mobility of ZnO is about 115–155 $cm^2\ V^{-1}\ s^{-1}$, which is much higher than that of TiO_2 and which is in the order of $1 \times 10^{-5}\ cm^2\ V^{-1}\ s^{-1}$ (Ganesh *et al* 2009) and also has the proper energy level for effective electron transfer from semiconductor nanoparticles (NPs) to the conduction band of ZnO after visible region irradiation (Hu and Chen 2007; Chen *et al* 2010). However, there are major limitations because of the poor absorption in the visible to near-infrared regions. Many efforts have been made to improve the potential to absorb a wider wavelength region.

Currently, semiconductor-sensitized solar cells (SSCs) have attracted much attention because of the improved properties of nanoparticle semiconductors over their bulkier counterpart such as a high extinction coefficient (Yu *et al* 2003), the large intrinsic dipole moment generated from the bulk properties of the semiconductor (Vogel *et al* 1990, 1994), multiple exciton production per photon through the impact ionization effect over conventional dyes under high energy excitation (Beard 2011), tunable absorption owing to the quantum confinement effect by size and shape control providing an excellent tool for the design of light absorbing materials (Alvisatos 1996; Kongkanard *et al* 2008), high stability and resistivity against photoblenching and atmospheric oxygen/water, and especially, the ability to be constructed as multilayered- or hybrid-sensitizers for a novel structure of semiconductor solar cells (Murray *et al* 2000; Kamat 2008). Most of the tailoring semiconductor sensitizers have been successfully synthesized by several groups, who have investigated characteristics and optical properties such as SnS (Miyauchi 2011), $Cu_{2-x}S$ (Lin and Lee

*Author for correspondence (tubtimtae@gmail.com)

2011), ZnTe (Chao *et al* 2010), $AgInS_2$ (Cheng *et al* 2011; Hamanaka *et al* 2011), Ag_2S (Tubtimtae *et al* 2010) and Ag_2Se (Tubtimtae *et al* 2011).

The tailoring transition-metal tellurides represent a class of compounds which is keenly sought for opto- and thermo-electric applications as these materials have high thermoelectric power values and doping ability for *n*- or *p*-types (Samal and Pradeep 2010).

Among these transition-metal tellurides, manganese telluride (MnTe) is one of the *p*-type semiconductors that we were interested in for use as a novel tailoring sensitizer because of its very high density of impurity charge carriers (Goswami and Mandale 1978), which can be used as a charge transport in a device. In addition, it has a narrow optical direct band gap of 1·3 eV (Oleszkiewicz *et al* 1988), which is close to the bulk direct band gap of SnS (E_g ~ 1·3–1·4 eV) (Potter and Simmons 1988; Panda *et al* 2006; Miyauchi 2011; Deepa and Nagaraju 2012), leading to high optical absorption and conductivity for photovoltaic applications (El-Nahass *et al* 2002). Recently, Santra and Kamat (2012) presented the first demonstrated strategy of transition metal–Mn^{2+} doping in single CdS and double-layered CdS/CdSe on a mesoporous TiO_2 photoanode yielding improved efficiencies for both devices of 2·53% and 5·42%, respectively, after Mn^{2+} doping. However, doping with metal elements was impaired by the thermal instability and induced more carrier recombinations in the cells. Consequently, doping with non-metal elements has been introduced to improve the photocatalytic efficiency, suppress the carrier recombination and modify its crystallization (Chen *et al* 2006). Previous literature, for instance, Luke *et al* (2008) have reported the synthesis of a CdSe semiconductor with nitrogen doping and has been deposited on a nanocrystalline TiO_2 film for use as a photoelectrode, which had a power conversion efficiency of 0·84% and it can be noted that combining nitrogen doping with the semiconductor sensitizer on TiO_2 thin films is an effective and promising procedure to enhance the photoresponse in the near-UV and visible region. Liu *et al* (2013) successfully synthesized carbon quantum-dot-doped CdS microspheres (C/CdS), where the C/CdS exhibited a crucial role in enhancing the photocatalytic activity, efficient charge separation and transportation in the composites and furthermore, a higher and more stabilized photocurrent density was generated.

Previously, the study of Grey *et al* (1996) suggested that boron (B^{3+})-incorporated semiconductor–metal oxide material could improve the photocatalytic activity and act as photogenerated electron traps to facilitate the charge separation and also play an important role to suppress the recombination between photogenerated electrons and holes in the electrolyte region. However, there has been a little study of boron doping in semiconductor sensitizing, until now. Therefore, we were interested in the use of boron as a dopant in a semiconductor sensitizer to modify the characteristics and the electronic and photophysical properties of a sensitizer and to create a trap state in the midgap region of a sensitizer, leading to an alteration of the charge separation and recombination dynamics and to report on the synthesis of boron-doped manganese telluride (B-doped MnTe) semiconductor-decorated ZnO nanoparticles by the SILAR process. Their characteristics, optical and photovoltaic properties were investigated for SSC application as a novel tailoring sensitizer.

2. Experimental

2.1 *Preparation of ZnO photoelectrode*

ZnO powder (< 100 nm, Aldrich) was mixed with polyethylene glycol (PEG, 20 wt%) and Triton X-100. The ratio of mixed materials to form a ZnO film was ZnO powder: PEG : Triton X-100 = 1 : 2 : 0·1 by weight and then, the solution was stirred for 30 min at room temperature. The ZnO photoelectrode was prepared by spreading on cleaned fluorine-doped tin oxide glass (FTO, 13 Ω cm^{-2}, Aldrich) using a doctor blade technique. The as-prepared sample was dried at 120 °C for 10 min, then fired at 400 °C for 1 h.

2.2 *Synthesis of B-doped MnTe sensitizer*

Non-metal B-doped MnTe sensitizer was synthesized on a ZnO photoelectrode through the two-step successive ionic layer adsorption and reaction (SILAR) process described below. First, Mn^{2+} ions were deposited on the ZnO surface by dipping the ZnO electrode into a precursor of 0·1 M $Mn(NO_3)_2$ with 0·075 M boron powder in ethanol solution for 1 min. Then, the electrode was rinsed thoroughly with ethanol and dried in air at 60 °C for 1 min. Subsequently, the electrode was dipped into 0·1 M Na_2O_3Te methanol solution for another 1 min as a precursor for Te^{2-} ions, after which it was rinsed with methanol and dried again in air at 60 °C for another 1 min. The entire process is referred to as one SILAR process. The MnTe(*n*) was referred to as *n* SILAR cycles of the dipping process. When the number of SILAR cycles was increased by dipping the ZnO electrodes in the solution with boron doping, the ZnO electrodes became more black-brownish, compared with an uncoated sample and the samples are shown in figure 1.

2.3 *Characteristics of B-doped MnTe sensitizer*

The structural characteristics of the B-doped MnTe were investigated using a high-resolution field emission scanning electron microscope (FESEM, JEOL JSM 7001F) with an energy dispersive X-ray spectroscope (EDS, INCA PentaFET × 3 Oxford). X-ray diffractometer (Model D8

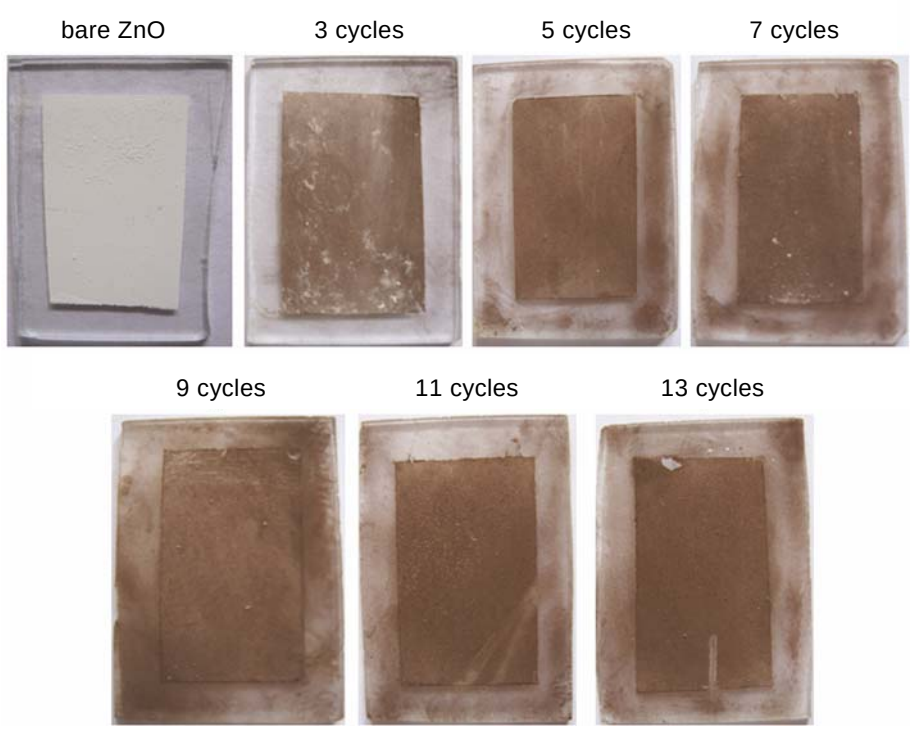

Figure 1. Characteristics of ZnO films after coating with various cycles of B-doped MnTe NPs.

Advance: Bruker AXS, Germany) was used to perform patterns of various conditions of photoelectrodes via CuKα radiation with a wavelength of 1·5406 Å, operated at 40 kV/30 mA from 20° to 80° and an increment of 0·01°. The scanning speed was 0·3 s per step and a transmittance electron microscope (HRTEM, FEI-Techni-20 G^2) operating at 200 kV. The ZnO film with the B-doped MnTe sensitizer coating was prepared on a TEM copper grid using the procedure described in the previous section.

2.4 *Assembly of B-doped MnTe semiconductor-sensitized ZnO photoelectrode*

The B-doped MnTe semiconductor-sensitized ZnO photoelectrode was assembled with Pt counterelectrode (Pt CE), prepared by 20 mM Cl_6H_2Pt dissolved in a mixed solution of acetone and 20% terpineol anhydrous and dropped on bare FTO glass, and then heated at 400 °C for 15 min. A 190 μm thick hot-melt parafilm was used as a spacer sealed between the photoelectrode and the counterelectrode. The iodide/triiodide (I^-/I_3^-) electrolyte consisted of 0·03 M I_2 and 0·3 M LiI was dissolved in propylene carbonate and was injected through a pin hole in the Pt CE and each hole was then sealed.

2.5 *Optical and photovoltaic properties*

The absorption spectra of various conditions were recorded using a UV–Vis spectrometer (Lambda 25, Perkin Elmer). The photovoltaic data were recorded under simulated sunlight from a solar simulator with radiant illumination of 100 mW/cm^2 (150 W Oriel Xe lamp with AM-1·5 filter) through a Keithley 2400 source meter. The incident light intensity was calibrated with a standard Si solar cell. The active area of the cell was 4 × 4 mm and a metal mask of size 4·5 × 4·5 mm was placed on top of the sample before recording the *I–V* measurements.

3. Results and discussion

Figure 2(a) shows the SEM images of bare ZnO nanoparticles and the B-doped MnTe semiconductor coated on the ZnO nanoparticles is shown in figure 2(b). Furthermore, in figure 2(c), the TEM micrograph shows clearly the B-doped MnTe nanoparticle characteristics deposited on the ZnO surface with a diameter of 15–30 nm. To confirm the deposition of B-doped MnTe semiconductors onto the ZnO surface, we investigated the EDS point analysis in figure 2(d) and the results showed the presence of manganese and tellurium on the ZnO surface; the stoichiometry based on the atomic ratio between the Mn and Te was approximately 1 : 1. The diffraction patterns in figure 3(a) show the ZnO signal before and after the B-doped MnTe coating. The signals of the two conditions looked similar and mainly show the ZnO signal, but the signal of ZnO after the B-doped MnTe coating was decreased. The resulting signal did not produce the peak of B-doped MnTe in the ZnO spectra due to the very

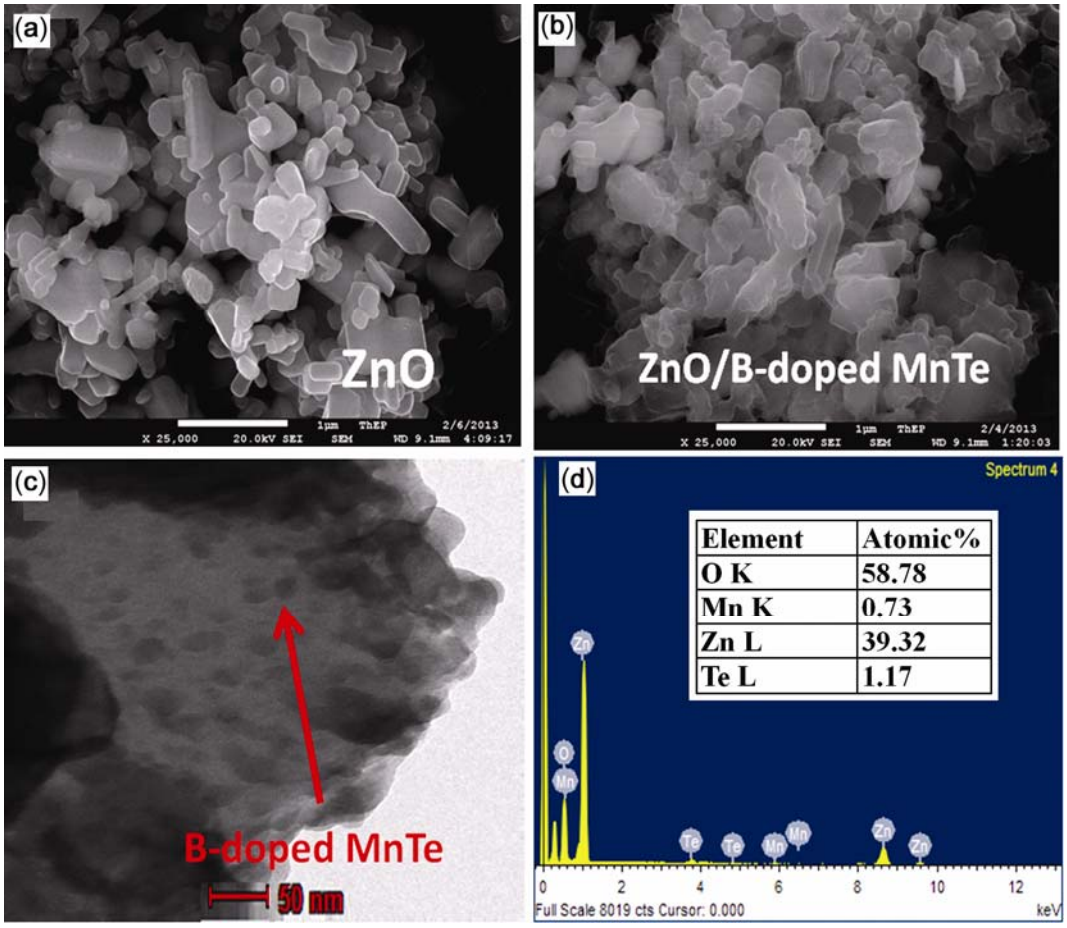

Figure 2. SEM images of (**a**) bare ZnO, (**b**) B-doped MnTe-coated ZnO, (**c**) TEM image of B-doped MnTe-coated ZnO and (**d**) EDS analysis and (inset) chemical elements of B-doped MnTe-coated ZnO nanoparticles.

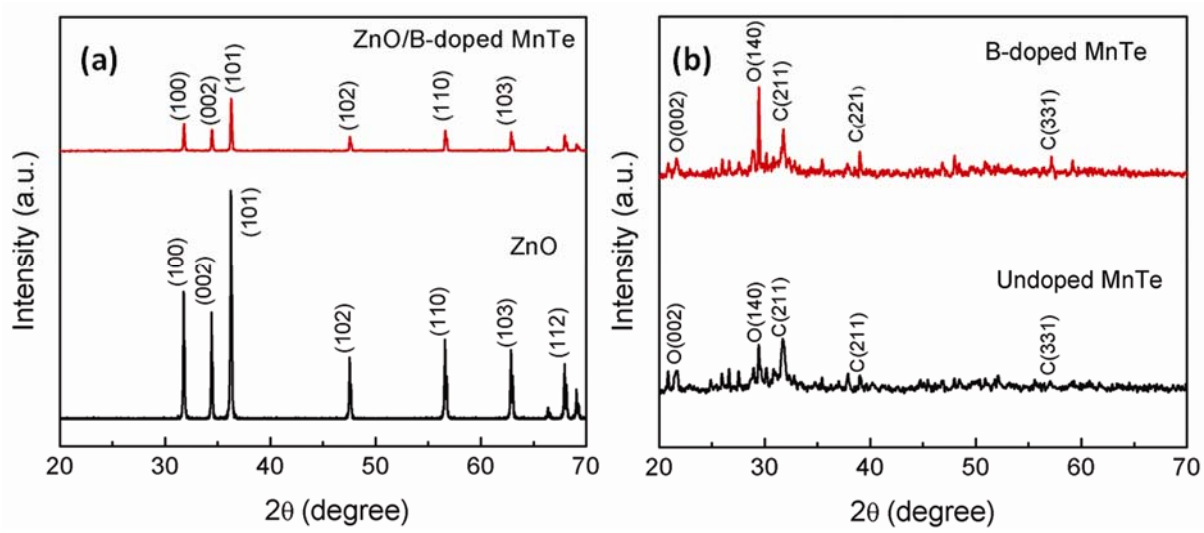

Figure 3. XRD patterns of (**a**) bare ZnO and B-doped MnTe-coated ZnO, and (**b**) comparison between undoped and B-doped MnTe NPs.

low intensity compared to that of the ZnO signal. The as-synthesized MnTe nanoparticles before and after boron doping in figure 3(b) confirm that the structure is crystalline. The mixed growth phases both before and after B-doped MnTe coating, i.e. orthorhombic MnTe at $2\theta =$ 21·707 (0 0 2) and 29·249 (1 4 0) (JCPDS no. 40-1195)

and cubic $MnTe_2$ at $2\theta = 31{\cdot}538$ (2 1 1) and 38·882 (2 2 1) (JCPDS no. 73-1526), agreed with the results of Sharma *et al* (2007). However, while both spectra look similar, the intensity of the (1 4 0), (2 2 1) and (3 3 1) peaks were higher due to the improvement in the crystalline quality and the larger size of crystal after boron doping.

Figure 4(a) shows the optical properties of absorption of bare ZnO, ZnO/undoped and B-doped MnTe NPs to support the crystal structures. The spectra showed that the samples had greater absorptivity to the incident light after the MnTe coating and in the B-doped MnTe structure. The plot of $(\alpha h\nu)^2$ vs $h\nu$ with various conditions was performed to determine the photon energy of the samples and showed the intercept of photon energy on the *X*-axis by extrapolating the linear line portion of the plot, producing values of 3·20 eV for bare ZnO, 1·30 eV for undoped MnTe NPs and 1·27 eV for B-doped MnTe NPs, which are in agreement with previous reports (Alvisatos 1996; Beard 2011). The narrower energy gap after boron doping was due to the larger size of the MnTe NPs deposited on the ZnO surface. Figure 4(b) shows the photovoltaic performance of various SILAR cycles of the B-doped MnTe NPs-deposited ZnO film. The short-circuit current density (J_{sc}) was 0·03–0·08 mA cm^{-2}, the open-circuit voltage (V_{oc}) was 0·17–0·37 V, the fill factor (*FF*) was 0·25–0·74 and the power conversion efficiency (η) was $3–14 \times 10^{-3}$%. The best η value of 14×10^{-3}% was yielded at $n = 11$ with $J_{sc} = 0{\cdot}07$ mA cm^{-2}, $V_{oc} = 0{\cdot}26$ V and $FF = 0{\cdot}74$. The undoped sample is shown for comparison in figure 5; the cell yielded a higher J_{sc} value of 0·13 mA cm^{-2} and lower V_{oc} and *FF* values of 0·14 V and 0·26, respectively, with an η value of 4×10^{-3}%. Hence, the power conversion efficiency of the boron-doped MnTe coated on the ZnO photoelectrode was increased by approximately 3·5 times or 250%, compared to that of the undoped sample. The percentage increase in the J_{sc} value and the percentage reduction in the V_{oc} value were 86% and 46%, respectively, while the *FF* value was reduced by 65% for the undoped sample, which arose from the large recombination of photogenerated electrons to the oxidized species at the photoelectrode and electrolyte interface (Goswami and Mandale 1978). There is little literature reporting the advantages of nonmetal–boron doping and interpreting the fact mechanism in figure 6, which is in such a good agreement with our results. The higher power conversion efficiency may be attributable to the trap state of boron doping as a midgap of MnTe NPs to facilitate the transfer of photogenerated electrons and low energetic electrons from the E_{CB} of MnTe to the E_{CB} of ZnO, leading to an increase in the photocatalytic

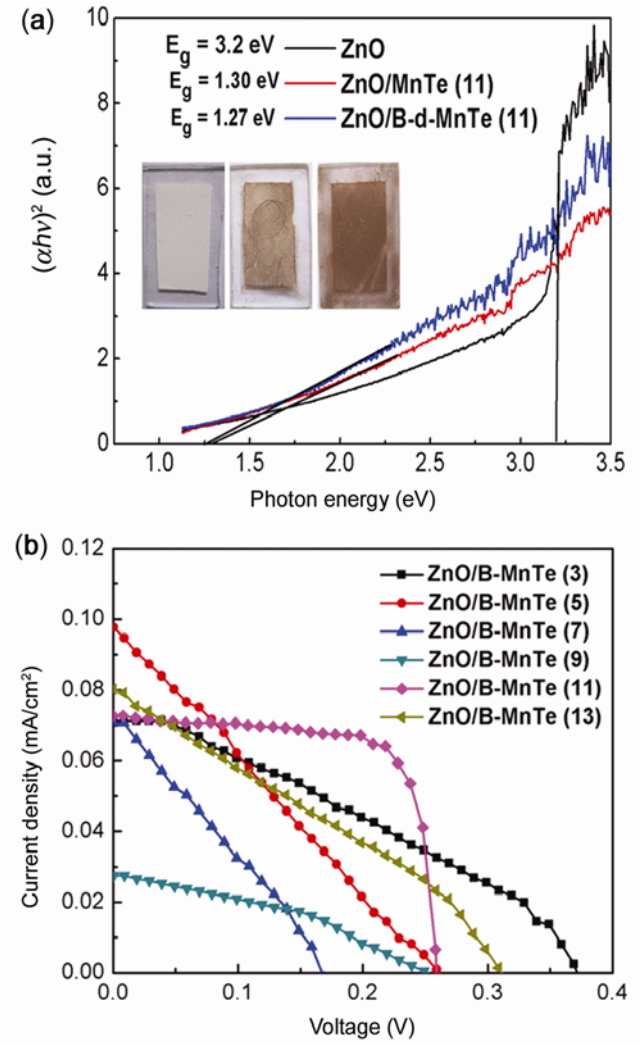

Figure 4. (**a**) Optical absorption characteristics and (**b**) *I–V* curves for B-doped MnTe-coated ZnO with various SILAR cycles.

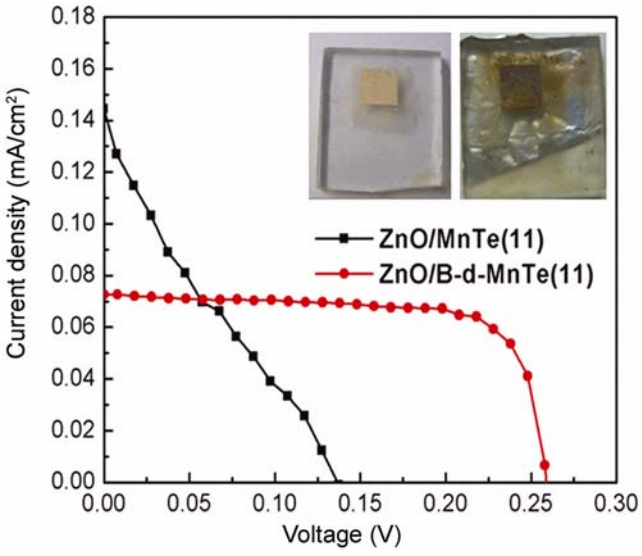

Figure 5. Comparison between undoped and B-doped MnTe-coated ZnO with optimal SILAR cycle ($n = 11$) measured under 100 mW cm^{-2} (AM 1·5 G).

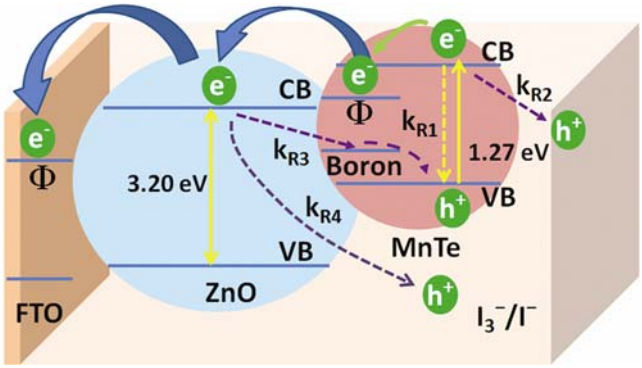

Figure 6. Schematic diagram of the carrier recombination and electron transfer process from B-doped MnTe into ZnO and through FTO.

activity and reduced carrier recombination inside the MnTe and between the MnTe/electrolyte interfaces (Grey *et al* 1996; Chen *et al* 2006). However, the low power conversion efficiency was considered to result from three components: (1) there are some regions of poor electrical contact between the B-doped MnTe NPs and the ZnO surface and between each ZnO NP due to the ZnO NPs not being spherical in shape, which leads to the low rectifying properties of the cell and it is difficult for the electrons to move in the external circuit, caused from the roughened surfaces of the photoelectrode; (2) although the midgap of boron at the MnTe will facilitate the transport of photogenerated and low energetic electrons on the E_{CB} of the MnTe and move forward to the E_{CB} of ZnO, there are still some carrier recombinations inside the MnTe structure (k_{R1}) and at the MnTe and electrolyte interface (k_{R2}); (3) there are no trap state mediator as a midgap to support electron transfer in the ZnO NPs; thus, it results in a high probability of carrier recombination at the E_{VB} of the MnTe (k_{R3}) and at the ZnO and electrolyte interface (k_{R4}).

4. Conclusions

We synthesized novel B-doped binary semiconductor MnTe NPs-sensitized ZnO solar cells using the SILAR technique. The energy gap of the MnTe sensitizer became narrower after boron doping, which is advantageous for broadening the absorption from the visible region to the NIR region and for improving its photocatalytic activity due to the suppression of carrier recombinations via a trap state in the MnTe structure, leading to higher power conversion efficiency. The low power conversion efficiencies produced in this research need to be improved by using an optimal material as a passivation layer or by further treatment to suppress carrier recombination. The research on this issue represents a stage in the improvement to produce higher power conversion efficiency and greater stability based on this type of semiconductor nanoparticle as a sensitizer.

Acknowledgements

We would like to acknowledge the Department of Physics and Research Promotion and Technology Transfer Center (RPTTC), Faculty of Liberal Arts and Science at Kasetsart University, Kamphaeng Saen Campus, for financial support and thanks to the Kasetsart University Research and Development Institute (KURDI) for critical proof reading. Moreover, Auttasit Tubtimtae and Suwanna Sheangliw would like to thank Applied Physics Research Laboratory (APRL), Department of Physics and Material Sciences, Faculty of Science at Chiang Mai University, for providing materials and measurement facilities.

References

Alvisatos A P 1996 *Science* **271** 933
Beard M C 2011 *J. Phys. Chem. Lett.* **2** 1282
Chao H Y, Cheng J H, Lu J Y, Chang Y H, Cheng C L and Chen Y F 2010 *Superlattices Microstruct.* **47** 160
Chen D, Yang D, Wang Q and Jiang Z 2006 *Ind. Eng. Chem. Res.* **45** 4110
Chen J, Wu J, Lei W, Song J L, Deng W Q and Sun X W 2010 *Appl. Surf. Sci.* **256** 7438
Cheng K C, Law W C, Yong K T, Nevins J S, Watson D F, Ho H P and Prasad P N 2011 *Chem. Phys. Lett.* **515** 254
Deepa K G and Nagaraju J 2012 *Mater. Sci. Eng.* **B177** 1023
El-Nahass M M, Zeyada H M, Aziz M S and El-Ghamaz N A 2002 *Opt. Mater.* **20** 159
Ganesh T, Mane R S, Cai G, Chang J H and Han S H 2009 *J. Phys. Chem.* **C113** 7666
Georgekutty R, Seery M K and Pillai S C 2008 *J. Phys. Chem.* **C112** 13563
Goswami A and Mandale A B 1978 *Jpn. J. Appl. Phys.* **17** 473
Grey I E, Li C and Macrae C 1996 *J. Solid State Chem.* **127** 240
Hamanaka Y, Ogawa T and Tsuzuki M 2011 *J. Phys. Chem. C* **115** 1786
Hu L and Chen G 2007 *Nano Lett.* **7** 3249
Kahn M L, Monge M, Collière V, Senocq F, Maisonnat A and Chaudret B 2005 *Adv. Funct. Mater.* **15** 458
Kamat P V 2008 *J. Phys. Chem.* **C112** 18737
Kongkanand A, Tvrdy K, Takechi K, Kuno M and Kamat P 2008 *J. Am. Chem. Soc.* **130** 4007
Lin M C and Lee M W 2011 *Electrochem. Commun.* **13** 1376
Liu Y, Yu Y X and Zhang W D 2013 *J. Alloys Compd.* **569** 102
Luke T L, Wolcott A, Xu L P, Chen S, Wen Z, Li J, Rosa E D L and Zhang J Z 2008 *J. Phys. Chem.* **C112** 1282
Majidi H and Baxter J B 2011 *Electrochim. Acta* **56** 2703
Miyauchi M 2011 *Chem. Phys. Lett.* **514** 151
Mu L X, Shi W S, Zhang T P, Zhang H Y, Wang Y, She G W, Gao Y H, Wang P F, Chang J C and Lee S T 2011 *Appl. Phys. Lett.* **98** 163101
Murray C B, Kagan C R and Bawendi M G 2000 *Annu. Rev. Mater. Sci.* **30** 545

Okazaki K, Kubo K, Shimogaki T, Nakamura D, Higashihata M and Okada T 2011 *Adv. Mater. Lett.* **2** 354
Oleszkiewicz J, Kisiel A and Ignatowicz S A 1988 *Thin Solid Films* **157** 1
Panda S K, Gorai S and Chaudhuri S 2006 *Mater. Sci. Eng.* **B129** 265
Potter Jr B G and Simmons J H 1988 *Phys. Rev.* **B37** 838
Ravirajan P, Peiró A M, Nazeeruddin M K, Gräetzel M, Bradley D D C, Durrant J R and Nelson J 2006 *J. Phys. Chem.* **B110** 7635
Samal A K and Pradeep T 2010 *J. Phys. Chem.* **C114** 1796
Santra P K and Kamat P V 2012 *J. Am. Chem. Soc.* **134** 2508
Sharma R K, Singh G, Shul Y G and Kim H 2007 *Physica* **B390** 314
Tubtimtae A, Lee M W and Wang G J 2011 *J. Power Sources* **196** 6603
Tubtimtae A, Wu K L, Tung H Y, Lee M W and Wang G J 2010 *Electrochem. Commun.* **12** 1158
Vogel R, Hoyer P and Weller H 1994 *J. Phys. Chem.* **98** 3183
Vogel R, Pohl K and Weller H 1990 *Chem. Phys. Lett.* **174** 241
Wang G, Yang X, Qian F, Zhang J Z and Li Y 2010 *Nano Lett.* **10** 1088
Yu W, Qu L, Guo W and Peng X 2003 *Chem. Mater.* **15** 2854
Zhu G, Lv T, Pan L, Sun Z and Sun C 2011 *J. Alloys Compd.* **509** 362